Effect of cellular interaction on glycolytic oscillations in yeast: a theoretical investigation

Jana WOLF and Reinhart HEINRICH[1]

Humboldt-Universität zu Berlin, Institut für Biologie, Theoretische Biophysik, Invalidenstrasse 42, D-10115 Berlin, Germany

On the basis of a detailed model of yeast glycolysis, the effect of intercellular coupling on the oscillatory dynamics is analysed theoretically. The model includes the main steps of anaerobic glycolysis, and the production of ethanol and glycerol. Transmembrane diffusion of acetaldehyde is included, since it has been hypothesized that this substance mediates the interaction. Depending on the kinetic parameters, the single-cell model shows both stationary and oscillatory behaviour. This agrees with experimental data with respect to metabolite concentrations and phase shifts. The inclusion of intercellular coupling leads to a variety of dynamical modes, such as synchronous oscillations, and different kinds of asynchronous behaviour. These oscillations can co-exist, leading to bi- and tri-rhythmicity. The corresponding parameter regions have been identified by a bifurcation analysis. The oscillatory dynamics of synchronized cell populations are investigated by calculating the phase responses to acetaldehyde pulses. Simulations are performed with respect to the synchronization of two subpopulations that are oscillating out of phase before mixing. The effect of the various processes on synchronization is characterized quantitatively. While continuous exchange of acetaldehyde might synchronize the oscillations for appropriate sets of parameter values, the calculated synchronization time is longer than that observed experimentally. It is concluded either that, in addition to the transmembrane exchange of acetaldehyde, other processes may contribute to intercellular coupling, or that intracellular regulatory feedback plays a role in the acceleration of the synchronization.

Key words: control coefficient, glycolysis, metabolic oscillations, phase response, synchronization.

INTRODUCTION

Glycolytic oscillations are one of the best studied examples of rhythmic behaviour on the cellular level. They occur in a broad spectrum of cells, e.g. in yeast, muscle, heart, and in pancreatic β-cells. The oscillations have been studied most extensively in suspensions and extracts of yeast cells. It was observed that all glycolytic intermediates oscillate with the same period, but with different phases, and that this period is in the range of 1 min (for recent reports, see [1,2]). The underlying oscillatory mechanism was found to be strongly dependent on the kinetic properties of the enzyme phosphofructokinase (PFK). This enzyme is highly regulated: it is activated by its substrate, fructose 6-phosphate, by its product, ADP and, in some cells, by its second product, fructose 1,6-bisphosphate. ATP acts at higher concentrations as an inhibitor, whereas AMP activates this enzyme. Theoretical models studying the occurrence of glycolytic oscillations are based on one or several of these regulatory effects. In addition to core models [3–5], more detailed models [6–8] have also been developed. Whereas the first group of models takes into account a feedback activation by either fructose 1,6-bisphosphate or ADP, the second group includes activatory and inhibitory effects of AMP and ATP respectively. The incorporation of adenine nucleotide concentrations as system variables necessitates the inclusion of ATP production in the second part of glycolysis, as well as of non-glycolytic, ATP-consuming processes (ATPases). It is generally thought that, in muscle cells, the generation of oscillations is due to the regulation of PFK by fructose 1,6-bisphosphate [8,9], whereas, in yeast, the same enzyme is mainly regulated by the adenine nucleotides.

In yeast cell suspensions the oscillations of glycolysis have been followed experimentally on the population level via monitoring mean concentrations, i.e. of NADH. In this way, only limited information has been obtained about the dynamics of a single cell within such a population [10]. Obviously, the existence of sustained oscillations on the population level implies that the individual cells also oscillate, and that the single cells are synchronized, at least to a certain extent. The existence of synchronizing interactions was also demonstrated directly by the mixing of two subpopulations that oscillate out of phase. In the resulting population, the oscillations are first damped, but reoccur after several cycles [11–13].

The models of glycolytic oscillations mentioned above are restricted to the case of single cells. The mathematical description of the effects of cellular coupling is still an open problem; in particular, for complex metabolic processes. A number of experiments, studying the nature of coupling, have suggested that cells interact by the exchange of a metabolic intermediate via the external medium. Ethanol, pyruvate and acetaldehyde have been discussed as candidates for the coupling metabolites [10,11,14]. Recent studies have yielded strong evidence that acetaldehyde mediates the coupling [13]. In particular, it was demonstrated that acetaldehyde is secreted by the cells, and that the extracellular concentration of this compound oscillates. Moreover, the cells respond to acetaldehyde pulses. These observations imply that the dynamics of a population are determined not only by the intracellular kinetics, but also by the exchange of substances between cells. The consequences of this hypothesis are addressed in the present theoretical study.

There are some indications that populations of cells do not always synchronize, but might also lose their synchrony [10]. This corresponds to theoretical results obtained for a two-component model, in which oscillations originate from a feedback-activation mechanism, and in which the effects of interactions within a population of identical cells were investigated in detail [15]. It was found that the transmembrane diffusion of a metabolite might lead to synchronized, as well as to desynchronized, states, depending on the values of the system parameters. In this basic model, two different types of asynchronous limit cycles may arise, corresponding (i) to regular asynchronous behaviour, where the amplitudes of the oscillating variables are the same in all cells and where the phase shifts between the cells are multiples of the reciprocal value of the number of cells, and (2) to non-regular asynchronous oscillations with non-identical oscillations in different cells and non-regular phase shifts. Simulations show that this dynamical behaviour might result in 'hidden oscillations', where large variations in the cellular concentrations are not represented by the corresponding mean values.

In the present study, we extend our analysis of intercellular communication to the case of glycolytic oscillations. To meet this aim, we have developed a detailed model for anaerobic energy metabolism in yeast cells. Compared with our previous investigations [15], we have arrived at a model comprising many variables for a single cell. A consideration of the coupling of these cells leads to a further increase of complexity, which can be analysed only by numerical methods. The identification of parameter regions with different dynamic behaviour was performed by bifurcation analysis using the software package AUTO [16].

THE MODEL

The reaction scheme

The starting point for our model is energy metabolism in yeast cells under anaerobic conditions, with the respiratory chain in a completely inhibited state and only alcoholic fermentation taking place. The reaction network of a single cell is represented by Scheme 1. It contains the main reactions of glycolysis, and adjacent reactions producing ethanol and glycerol.

The individual processes in Scheme 1 are shown to represent the following: flux 0 (J_0), input of glucose via the cellular membrane; reaction 1 (where the reactions are shown in the Scheme by v_1, v_2, etc.), lumped reactions of hexokinase, phosphoglucoisomerase and PFK; reaction 2, glyceraldehyde-3-phosphate dehydrogenase reaction; reaction 3, lumped reactions of phosphoglycerate kinase, phosphoglycerate mutase, enolase and
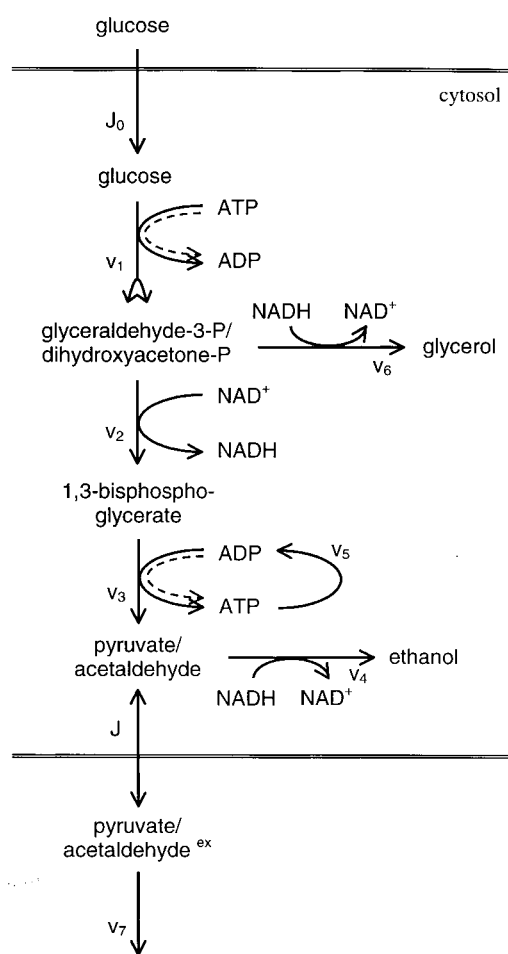
Scheme 1   Reaction scheme for a single cell

The scheme shows the main reactions of anaerobic glycolysis in yeast, in addition to transmembrane transport of glucose and the coupling substance (pyruvate and/or acetaldehyde). For further details and explanation of the symbols used, see the text.

pyruvate kinase; reaction 4, alcohol dehydrogenase reaction; reaction 5, non-glycolytic ATP consumption; reaction 6, formation of glycerol from triose phosphates; and reaction 7, degradation of the coupling substance in the extracellular medium. Furthermore, the model includes the membrane transport of the coupling substance, characterized by the flux, J.

A_3 and A_2, and N_1 and N_2 denote the concentrations of ATP and ADP, and NAD^+ and NADH, respectively. Owing to the fact that several glycolytic reactions are omitted and that other reactions are lumped, the model variables denote, in some cases, the concentrations of pools of intermediates, rather than concentrations of individual compounds. This concerns the pool of the triose phosphates, glyceraldehyde 3-phosphate and dihydroxyacetone phosphate (variable S_2), and the pool of pyruvate and acetaldehyde (variable S_4). The concentration of glucose is represented by the variable S_1, and that of 1,3-bisphosphoglycerate by S_3. Furthermore, the lumping process implies that the concentrations of some compounds do not appear as separate model variables. Such a reduction in model complexity may be justified by quasi-steady-state approximations for the concentration of metabolites located between the lumped reactions, as shown in detail previously [17].

In Scheme 1, the broken arrows in reactions 1 and 3 indicate that, in these lumped reactions, two molecules of the adenine nucleotides are converted, which corresponds to the overall stoichiometry of glycolysis. In reaction 1, two molecules of S_2 are produced (denoted by the arrow with two heads), corresponding to the splitting of a hexose phosphate into triose phosphates.

S_4^{ex} denotes the concentration of the coupling substance in the external solution. According to the definition of the pool compound S_4, it represents pyruvate and/or acetaldehyde. This corresponds to experimental results [13], which strongly suggest that acetaldehyde is the coupling metabolite. It was shown that cyanide produces, in addition to the inhibition of respiration, a second effect; that is, the partial removal of acetaldehyde [13]. Therefore an external degradation of the coupling substance due to the reaction of acetaldehyde with cyanide to yield lactonitrile is included in the present model.

Mathematical description

The reaction rates are denoted by v_j^α, where the reactions are numbered by the subscript j and the cells are numbered by the superscript α. The irreversible input flux of glucose and the reversible transmembrane flux of the coupling substance are denoted by J_0^α and J^α respectively. The latter flux is counted positive if it is directed from the intra- to the extra-cellular medium. The kinetic equations, characterizing the functional dependence of the reaction rates on the metabolite concentrations, are assumed to have the same form for all cells. Furthermore, the cells are identical with respect to the kinetic parameters. All reactions, as well as their input, are considered to be irreversible. The reaction rates are described by linear and bilinear functions of the concentrations of their substrates, except for the first reaction (lumped reaction of hexokinase and PFK), where inhibition by ATP, according to the substrate inhibition of PFK, is additionally taken into account. In detail, the kinetic equations read:

$$v_1 = k_1 S_1 A_3 f(A_3), \text{ with } f(A_3) = \left[1 + \left(\frac{A_3}{K_I}\right)^q\right]^{-1} \tag{1a}$$

$$v_2 = k_2 S_2 N_1 \tag{1b}$$

$$v_3 = k_3 S_3 A_2 \tag{1c}$$

$$v_4 = k_4 S_4 N_2 \tag{1d}$$

$$v_5 = k_5 A_3 \tag{1e}$$

$$v_6 = k_6 S_2 N_2 \tag{1f}$$

$$v_7 = k S_4^{ex} \tag{1g}$$

To obtain from equation system (1) the reaction rates v_i^α for a given cell α, one has to introduce the metabolite concentrations in that cell. k_j $(j = 1, \ldots, 6)$ and k are rate constants; K_I and q are the inhibition constant and the co-operativity coefficient of the ATP inhibition respectively. For the transmembrane fluxes, we use:

$$J_0 = \text{constant} \tag{2a}$$

$$J^\alpha = \kappa(S_4^\alpha - S_4^{ex}) \tag{2b}$$

where the kinetic constant κ is related to the permeability (P) of the membrane for the coupling substance S_4 by the equation:

$$\kappa = A_s P/V \tag{2c}$$

where A_s represents the membrane surface and V is the cellular volume.

We assume that the intracellular metabolites are distributed homogeneously in each cell, and the exchangeable ones in the external solution. The latter assumption corresponds to the experimental situation of a well-stirred solution. The differential equation system of the model for n coupled cells reads:

$$\frac{dS_1^\alpha}{dt} = J_0 - v_1^\alpha \tag{3a}$$

$$\frac{dS_2^\alpha}{dt} = 2v_1^\alpha - v_2^\alpha - v_6^\alpha \tag{3b}$$

$$\frac{dS_3^\alpha}{dt} = v_2^\alpha - v_3^\alpha \tag{3c}$$

$$\frac{dS_4^\alpha}{dt} = v_3^\alpha - v_4^\alpha - J^\alpha \tag{3d}$$

$$\frac{dN_2^\alpha}{dt} = v_2^\alpha - v_4^\alpha - v_6^\alpha \tag{3e}$$

$$\frac{dA_3^\alpha}{dt} = -2v_1^\alpha + 2v_3^\alpha - v_5^\alpha \tag{3f}$$

$$\frac{dS_4^{ex}}{dt} = \frac{\varphi}{n} \sum_{\alpha=1}^{n} J^\alpha - v_7 \tag{3g}$$

where $\alpha = 1, \ldots, n$. Therefore the model for a population of n cells contains $(6n + 1)$ variables. The differential equations for N_1^α and A_2^α are omitted, since these concentrations follow from the conservation conditions:

$$N_1^\alpha + N_2^\alpha = N = \text{constant} \tag{4a}$$

$$A_2^\alpha + A_3^\alpha = A = \text{constant} \tag{4b}$$

φ denotes the ratio of the total cellular volume, $V_C = nV$, to the extracellular volume, V_E.

STEADY STATES

The model for a population of n cells has a symmetric steady state, characterized by identical sets of stationary metabolite concentrations for all cells. These concentrations are the same as

Table 1 Parameter values of the reference state

Parameter	Value
J_0	3.0 mM·min^{-1}
k_1	100.0 mM^{-1}·min^{-1}
k_2	6.0 mM^{-1}·min^{-1}
k_3	16.0 mM^{-1}·min^{-1}
k_4	100.0 mM^{-1}·min^{-1}
k_5	1.28 min^{-1}
k_6	12.0 mM^{-1}·min^{-1}
k	1.3 min^{-1}
κ	13.0 min^{-1}
q	4.0
K_I	0.52 mM
N	1.0 mM
A	4.0 mM
φ	0.1

Table 2   Stationary concentrations in the reference state

Metabolite	Concentration (mM)
S_1	5.8
S_2	0.9
S_3	0.2
S_4	0.2
N_2	0.1
A_3	2.4
S_4^{ex}	0.1

Figure 1   Bifurcation diagram of the NADH concentration for a single cell

Shown are the steady-state values and the maxima and minima of the oscillations for the variable N_2 at different values of the bifurcation parameter, k. Parameter values of the bifurcation points: $k_H = 1.38$ min^{-1}, $k_L = 0.49$ min^{-1}. H and L denote a Hopf bifurcation and a saddle-node bifurcation respectively. Open circles represent an unstable limit cycle; filled circles show stable limit cycles.

in the case of a single cell. Despite the non-linearity of the algebraic steady-state equations, an explicit solution can be found (see Appendix A).

The reference state of the model is defined by the combination of kinetic parameters listed in Table 1, and the corresponding stationary concentrations of metabolites are given in Table 2. The parameter values of that reference state have been selected in such a way that the metabolite concentrations are in a realistic range for yeast cells [2]. For most investigations presented below, the parameters are fixed to their reference values, except J_0, φ and k, which are treated as bifurcation parameters. This choice is dictated by the fact that the input flux, the cell density and the rate of degradation of the coupling substance are under experimental control.

For $n > 1$, in addition to eqns. (A1)–(A7) (see Appendix A), there are further solutions of the steady-state equation system, with non-identical values of the corresponding variables in different cells. In all cases studied, one or more concentration variables become negative; therefore, these mathematical solutions have no biochemical meaning.
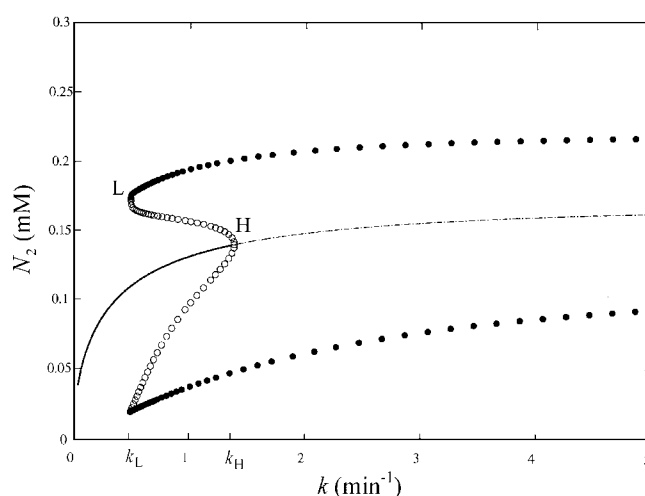
The stability of the symmetric steady state of n interacting cells was analysed by linearization of the system eqns. (1)–(4) in the vicinity of the steady state given in eqns. (A1)–(A7). As shown in Appendix B, the characteristic polynomial of the eigenvalues λ of the Jacobian may be factorized for $n > 1$ into two parts, such that:

$$F(\lambda) \cdot D(\lambda)^{n-1} = 0 \qquad (5)$$

The factor $F(\lambda)$ corresponds to the polynomial of the single cell, and is therefore of seventh degree. The other factor, $D(\lambda)$, appearing in the power of $(n-1)$, is of sixth degree. The possibility of such a factorization was also demonstrated in the minimal model [15]. The solutions of eqn. (5) determine the stability of the stationary state. In the region of instability, we observed oscillations in the case of a single and many cells.

DYNAMICS OF A SINGLE CELL

We first studied the dynamics of a single cell by determining the system behaviour as the parameter k is varied. This led to the bifurcation diagram for the concentration of NADH (variable N_2) in Figure 1. All parameters, except k, take the values of the reference set (Table 1). The steady state is stable (continuous line) for small k values (low external degradation rates of acetaldehyde) and unstable (broken line) for higher values of this parameter. Filled circles and open circles indicate the amplitudes of stable and unstable limit cycle oscillations respectively. The point H indicates a Hopf bifurcation, which follows from the roots of the characteristic polynomial given in eqn. (5), which, for $n = 1$, is reduced to $F(\lambda) = 0$. The bifurcation is subcritical, i.e. an unstable limit cycle originates from the steady-state branch. The limit cycle becomes stable at the point L. In the

region $k_L \leqslant k < k_H$, a stable steady state co-exists with a stable limit cycle, whereas, for $k_H \leqslant k$, a limit cycle is the unique stable solution. Figure 2 shows the oscillation period T in the same range of k as that used in Figure 1. The period decreases from 1.8 min to about 1.2 min if k is increased from 0.49 to 5.0 min^{-1}. This range for the period is comparable with the experimental values [2,18].

Experimental data indicate that the oscillating cellular metabolite concentrations have characteristic phase shifts. In particular, the following pairs of variables, ATP/ADP, NAD$^+$/NADH, ATP/NADH and fructose 6-phosphate/fructose 1,6-bisphosphate, oscillate 180° out of phase. Furthermore, glucose 6-
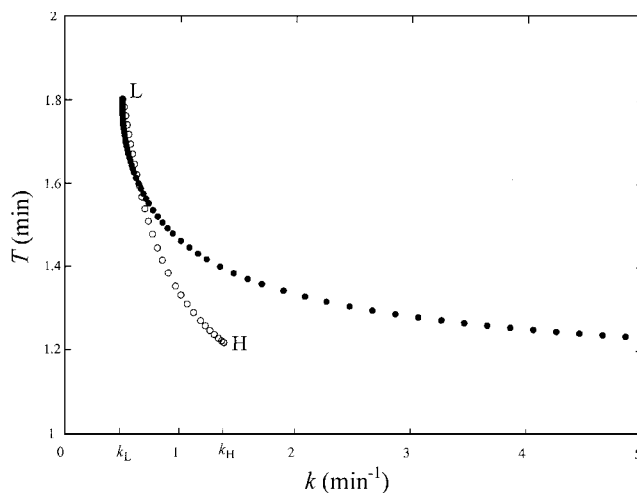
Figure 2   Bifurcation diagram of the oscillation period for a single cell

Period T of the limit cycle oscillations as a function of k for the same parameter range as in Figure 1.

phosphate and fructose 6-phosphate, as well as AMP and ADP, oscillate in phase, and the phase shift of fructose 1,6-bisphosphate and NADH is 70° [2].

Numerical integrations for $k > k_L$ revealed that the phase shift of ATP and NADH is well reproduced by our model. This also includes the anti-phase relation of ATP/ADP, and that of NAD^+/NADH, which, however, are direct consequences of the conservation conditions (eqns. 4a and 4b). The substrate S_1 and the product S_2 of the regulated reaction 1 oscillate almost in anti-phase, which show some correspondence to the out-of-phase oscillation of the substrate (fructose 6-phosphate) and product (fructose 1,6-bisphosphate) of PFK.

TWO INTERACTING CELLS: BIFURCATION ANALYSIS AND DYNAMICAL BEHAVIOUR

Figure 3 shows a schematic representation of the bifurcation diagram of two coupled cells by using, again, k as bifurcation parameter. This scheme is valid for all metabolites, since the type of the dynamical behaviour, i.e. whether it is a steady-state or an oscillatory state, is the same for all variables for any given value of k. Figure 3 demonstrates the rich repertoire of dynamics for the given system. It provides the correct picture concerning the succession of the bifurcations with respect to parameter k. The amplitudes of the variable were plotted in such a way that the most simple arrangement was obtained. Details of the original bifurcation diagram are shown for the variable A_3 in Figures 4 and 5.

The steady state (straight line) in Figure 3 is stable for $k < k(H_{syn})$ (continuous line) and unstable otherwise (broken line).

The stability changes via a Hopf bifurcation, resulting from the factor $F(\lambda)$, such that $k(H_{syn})$ has the same value as k_H of the single cell. In the two-cell model a second Hopf bifurcation results from the factor $D(\lambda)$, and occurs at $k(H_{asyn})$ on the unstable branch of the symmetric steady state. Both Hopf bifurcations are subcritical, and the two curves originating from the corresponding points represent amplitudes of unstable limit cycles. At decreasing k values, both limit cycles become stable at L_{syn} and L_{asyn} respectively, leading either to synchronous oscillations (phase shift $\tau = 0$ between the cells) on branch b1 or to regular asynchronous oscillations ($\tau = T/2$) on branch b2. In both cases, the cells oscillate with identical amplitudes. Branches b1 and b2 become unstable at the symmetry breaking bifurcation points B1 and B2 respectively. Figures 6(A) and 6(B) show an example of regular asynchronous oscillations corresponding to branch b2 for the concentration of ATP. In a region where the synchronous and the regular asynchronous oscillations are unstable, a stable branch b4 exists on which the two coupled cells oscillate with slightly different amplitudes and with a phase shift $0 < \tau < T/2$ (non-regular asynchronous oscillations; for an example, see Figures 7A and 7B). Beyond B3 the only stable states are synchronous oscillations.

In addition to branch b4, there exists a second branch connecting the synchronous and the regular asynchronous oscillations. This branch (b5) originates in B1, and also represents non-regular asynchronous oscillations. In contrast with b4, branch b5 has a stable and an unstable part. Another higher bifurcation in B5 leads, via an unstable part, to the stable branch b6 at $k(L_k)$. As found for b4, the amplitudes of the oscillations on the branches b5 and b6 are different for the two cells. In contrast
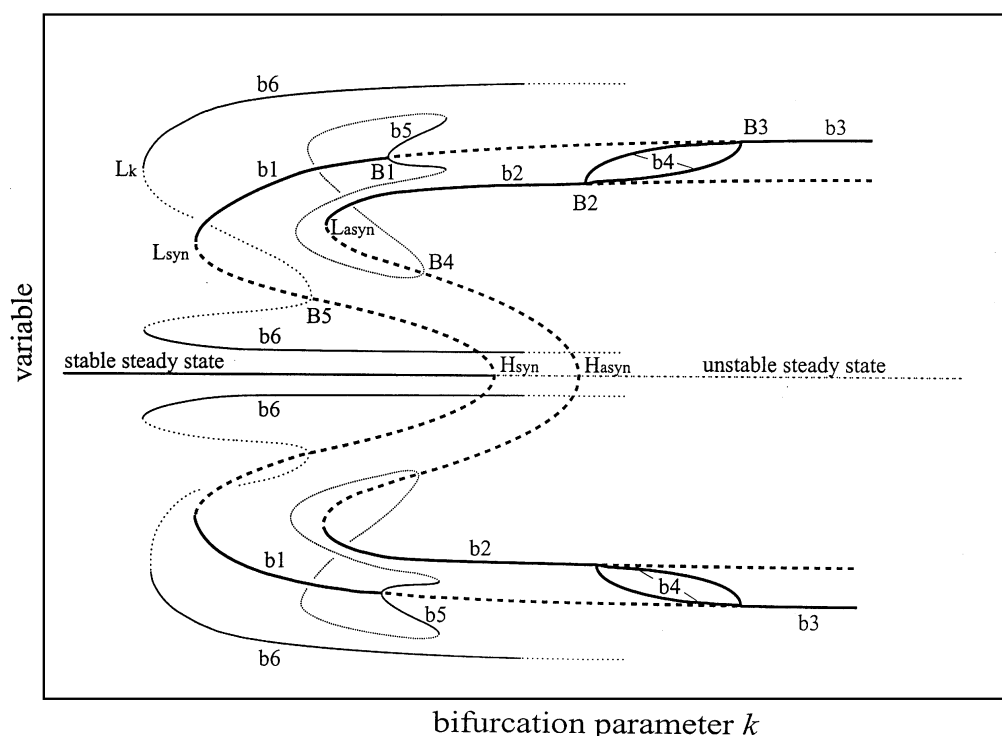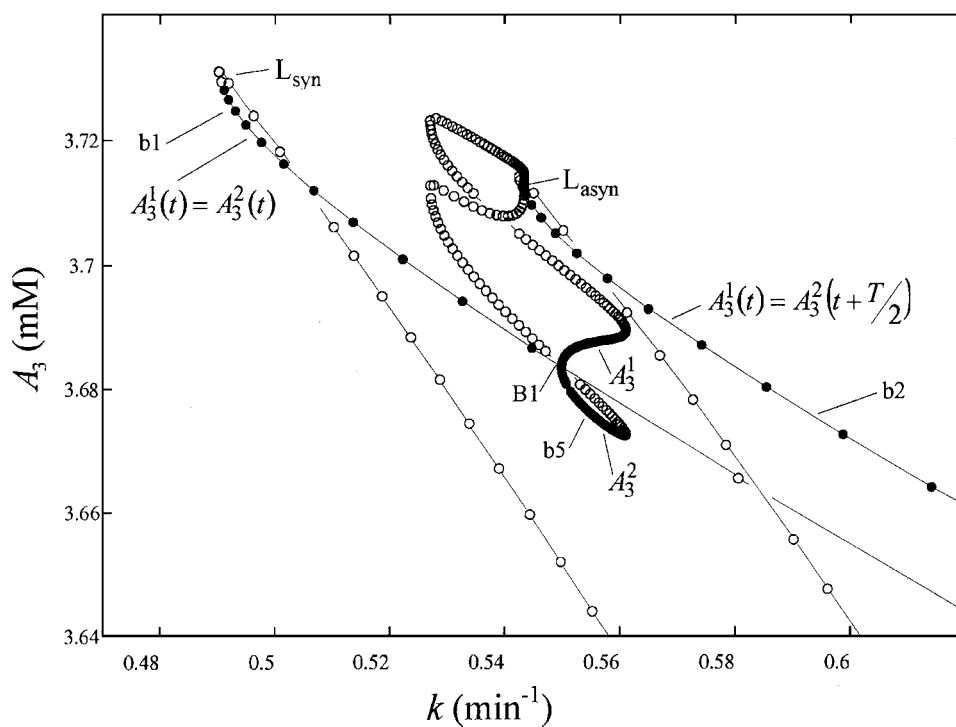

Figure 3   Schematic bifurcation diagram for two coupled cells

Continuous and broken lines represent, respectively, stable or unstable stationary or oscillatory states for the system variables at different values of the bifurcation parameter k. H_{syn} and H_{asyn} denote subcritical Hopf bifurcations. At L_{syn}, L_{asyn} and L_k saddle-node bifurcations of limit cycles occur. Branches b1–b6 represent the amplitudes (maxima and minima) of stable limit cycles. On b1, b2 and b3, the amplitudes of the given compound are identical in the two cells. On branches b4, b5 and b6, the cellular metabolites differ in their amplitudes. Branch b6 is characterized by high amplitudes in one cell and low amplitudes in the other cell. Points B1 to B5 represent symmetry breaking bifurcation points of higher order.
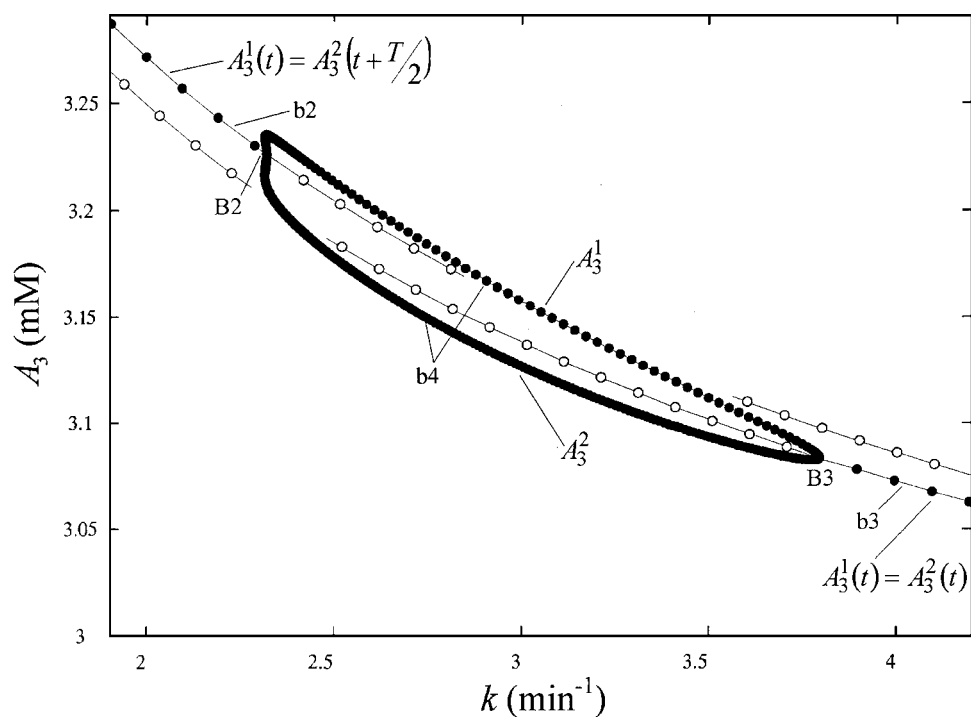
Figure 4   **Bifurcation diagram for the ATP concentrations A_3^1 and A_3^2 for high values of the bifurcation parameter k**

The diagram shows parts of branches b2, b3 and b4 introduced schematically in Figure 3.

Figure 5   **Bifurcation diagram for the ATP concentrations A_3^1 and A_3^2 for low values of the bifurcation parameter k**

The diagram shows parts of branches b1, b2 and b5 introduced schematically in Figure 3. Despite the fact that the stable branch b5 and its unstable continuation look more complicated in this original calculation than in the schematic picture, their topological structures do not differ. Branches b1 and b2 become stable slightly behind the bifurcation points L_{syn} and L_{asyn} respectively, a detail which is not shown in Figure 3.
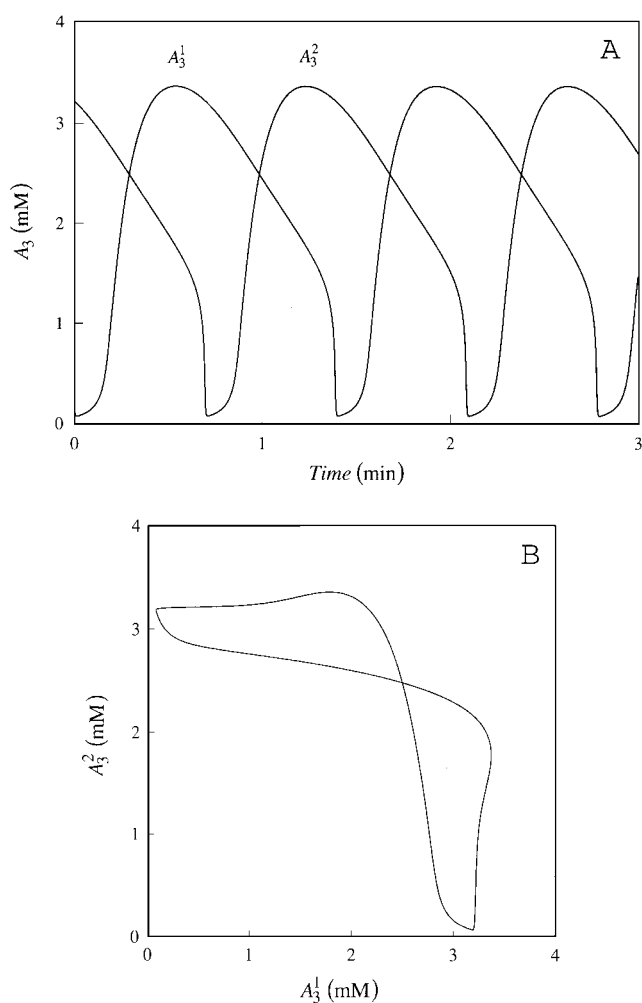
Figure 6   Regular asynchronous oscillation of the ATP concentrations A_3^1 and A_3^2 in two interacting cells corresponding to branch b2 of Figure 3 for $k = 1.5$ min^{-1}; other parameters are as given in Table 1

The amplitudes are identical for both cells ($\Delta A_3^1 = \Delta A_3^2 = 3.29$ mM) and the phase shift is $\tau = T/2$ with $T = 1.39$ min. (**A**) temporal development; (**B**) phase plane representation.
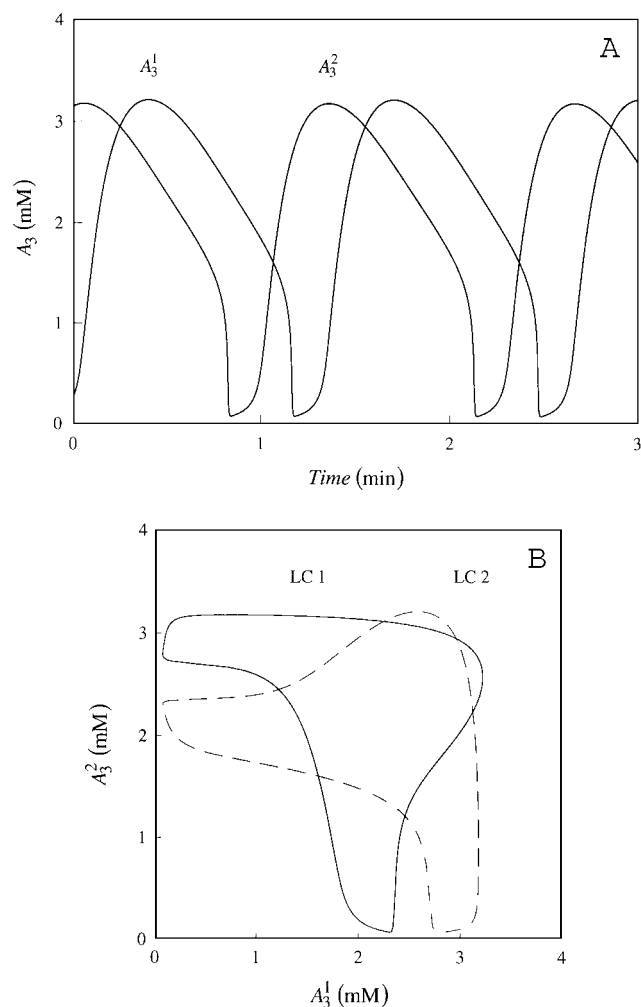
Figure 7   Non-regular asynchronous oscillations of the ATP concentrations A_3^1 and A_3^2 in two coupled cells corresponding to branch b4 of Figure 3 for $k = 2.5$ min^{-1}; other parameters are as given in Table 1

The amplitudes are non-identical ($\Delta A_3^1 = 3.11$ mM, $\Delta A_3^2 = 3.14$ mM). Period of the oscillation: $T = 1.30$ min; phase shift between the cells $\tau = 0.34$ min $\neq T/2$. (**A**) temporal development; (**B**) phase plane representation. The solid curve LC1 in (**B**) represents the limit cycle corresponding to the oscillation shown in (**A**); the broken curve is a second limit cycle LC2, which occurs for reasons of symmetry.

with the oscillations in Figure 7 (branch b4), where the amplitudes of the two cells differ only slightly, the oscillations of branch b6 shown in Figures 8(A) and 8(B) are characterized by high amplitudes in one cell and very low amplitudes in the other cell.

Figure 3 reveals that there exist parameter regions where different stable oscillatory modes may be reached, depending on the initial conditions. The simultaneous existence of the stable parts of branches b1 and b6 at low k values indicates the occurrence of bi-rhythmicity in the present model. At higher k values (beyond the bifurcation L_{asyn}) there exists even a 'tri-rhythmicity' of a synchronous oscillation and two different kinds of asynchronous oscillations, or, alternatively (beyond B1), of three types of asynchronous behaviour.

Figures 4 and 5 give detailed results for branches b4 and b5, and for the maxima of the oscillations for the variable A_3. Branch b4 shown in Figure 4 consists of an upper part, representing the maxima of the amplitudes of A_3 in cell 1, and a lower part for A_3 in cell 2, such that the variations of ATP in cell 1 are more pronounced than in cell 2. The phase shift between the two cells decreases continuously at increasing values of k from $\tau = T/2$ to

$\tau = 0$, which is in line with the fact that b4 connects regular asynchronous and synchronous oscillations. Because of the symmetry, branch b4 also represents a second stable limit cycle, where the roles of cell 1 and cell 2 are exchanged.

Figure 5 shows branches b1 and b5 in detail, as well as a part of b2. The branch b5 originates from the stable branch b1 at the point B1 by a supercritical bifurcation. The unstable continuation of b5 leads to bifurcation point B4, which is located on the unstable branch of regular asynchronous oscillations.

The main bifurcations H_{syn}, H_{asyn}, L_{syn}, L_{asyn} and L_k explained above are represented in Figure 9, where, in addition to k, the parameter J_0 is varied. For $n = 1$, the lines H_{asyn}, L_{asyn} and L_k do not exist, whereas the lines H_{syn} and L_{syn} are independent of the number of cells. These bifurcation lines divide the (k, J_0)-plane into different regions. In the region left of the lines L_{syn}, L_{asyn}, or L_k, the system will always approach a stable steady state. In the grey-shaded region on the right of H_{syn}, the stationary state is
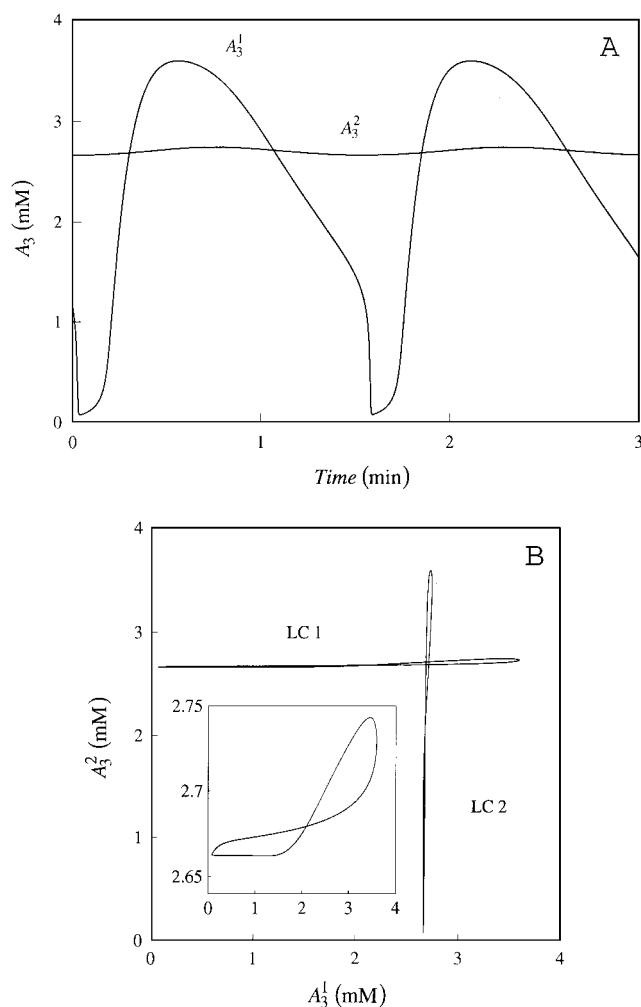
Figure 8   Non-regular asynchronous oscillations of the ATP concentrations A_3^1 and A_3^2 in two interacting cells corresponding to branch b6 of Figure 3 for $k = 0.7$ min^{-1}; other parameters are as given in Table 1

The amplitudes differ greatly ($\Delta A_3^1 = 3.52$ mM, $\Delta A_3^2 = 0.08$ mM). The period of the oscillation $T = 1.55$ min; phase shift between the maxima of the oscillations $\tau = 0.20$ min $\neq T/2$. (**A**) temporal development; (**B**) phase plane representation. Limit cycle LC1 corresponds to the oscillation shown in (**A**); a second limit cycle LC2 occurs for reasons of symmetry. Inset: detailed phase plane representation of LC1.

unstable and the system will tend towards one of the limit cycles representing synchronous, regular asynchronous or non-regular asynchronous oscillations. In the region left of H$_{syn}$ and right of the other bifurcation lines, the system reaches eventually the stable steady state or one of the possible limit cycles. The thin straight line corresponds to the parameter variation performed for the bifurcation analysis in Figures 3–5. From Figure 9 it becomes clear that, for higher values of J_0, the sequence of the bifurcations L$_{syn}$, L$_{asyn}$ and L$_k$ differs from that described above for $J_0 = 3.0$ mM·min^{-1}.

The diagram presented in Figure 9 shows some agreement with experimental data. (1) As shown in [19], there is a lower limit in the degradation rate of the coupling substance in the external medium (characterized by the parameter k) for the induction of glycolytic oscillations in yeast cell populations. This is in agreement with our theoretical result that, for low k values, only stable steady states exist. (2) Glycolytic oscillations are observed in

extracts and suspensions of yeast cells only in a limited range of the input flux of glucose (represented in the model by J_0). Below a critical value J_0, as well as for high values of the influx, no limit cycle oscillations are possible in experiments, a result which is clearly reflected by the diagram given in Figure 9.

The analysis may be extended further by the consideration of other bifurcation parameters. In accordance with the experimental data, there exists in our model an upper limit of the cell density φ for the occurrence of oscillations (results not shown). There is no bifurcation line giving a lower limit of that parameter for the occurrence of oscillations. However, the time to synchronize the population becomes greatly lengthened at low densities, which may explain why no oscillations are observed under these circumstances in the experiments [18].

CELL POPULATIONS

The Hopf bifurcations leading to synchronous and asynchronous limit cycles are independent of the number n of interacting cells (see Appendix B). Moreover, numerical investigations show that these bifurcations are subcritical, not only for $n = 2$ (H$_{syn}$ and H$_{asyn}$ in Figures 3 and 9), but also for higher numbers. Saddle-node bifurcations of limit cycles (L$_k$, L$_{syn}$ and L$_{asyn}$ in Figures 3 and 9) exist also for $n > 2$. These similarities in the bifurcations of systems with different cell numbers lead to the general occurrence of synchronous oscillations, regular asynchronous oscillations and non-regular asynchronous oscillations. In the regular asynchronous state all cells oscillate in an identical way, but with fixed phase shifts, which are multiples of $\tau = T/n$. Accordingly, the external concentration of the coupling substance shows oscillations, the amplitudes of which are significantly smaller compared with the synchronous state.

Phase response after addition of acetaldehyde

An appropriate way to investigate the effect of a substance on an oscillating system is by perturbation experiments. Experimentally, this was investigated for pulses of acetaldehyde given to the external medium of a yeast suspension [13,14]. This choice was encouraged by the idea that a metabolite which couples the individual cells should be able to affect the intracellular oscillatory dynamics. Acetaldehyde was found to induce phase shifts, depending on the initial change of the acetaldehyde concentration, as well as on the phase where the perturbation is applied.

According to the experimental situation the phase response $\Delta\Psi$ of NADH was investigated. Perturbations were applied to a suspension of synchronized cells at different phases Φ within one period. The angles are measured in such a way that $\Phi = 90°$ indicates that the pulse of acetaldehyde is applied when the NADH concentration attains its maximum, corresponding to the choice of the co-ordinate system used in experimental studies [13].

Figure 10 shows an example of the time course of acetaldehyde and NADH, where a pulse of 0.2 mM acetaldehyde is applied shortly after the maximum of NADH ($\Phi = 110°$). The simulation was performed for $J_0 = 2.5$ mM·min^{-1}, $k = 1.8$ min^{-1}, with reference values for all other parameters (for this combination of parameter values, only the synchronous oscillation was a stable solution). Before the pulse, the NADH concentration oscillated between 0.08 and 0.2 mM, and the external concentration of acetaldehyde was in the range 0.05 to 0.1 mM with a period of $T = 1.17$ min. After the pulse, the first maximum occurred after a period $T = 1.25$ min, which corresponded to a phase shift $\Delta\Psi_1 =$
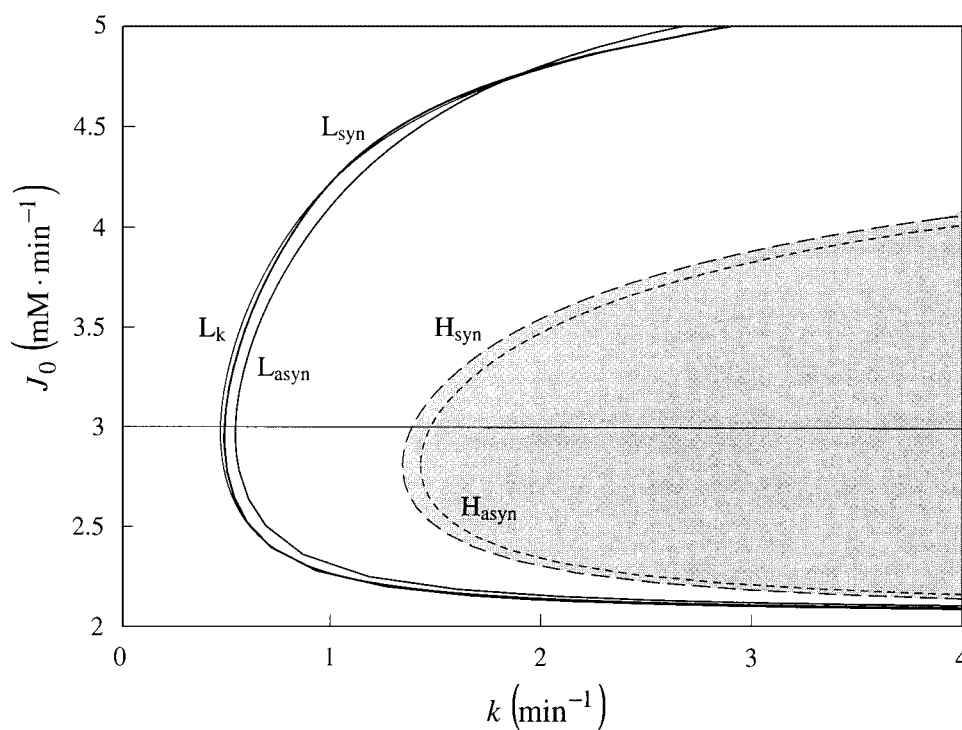
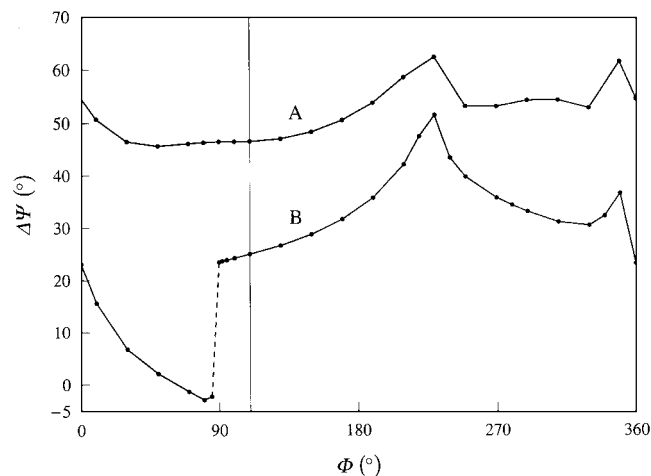**Figure 9   Bifurcation lines in the parameter plane (k, J_0)**

Whereas H_{syn} and H_{asyn} denote Hopf bifurcation lines; L_{syn}, L_{asyn} and L_k give the points of saddle-node bifurcations. The thin straight line corresponds to the parameter variation performed for the bifurcation analysis in Figures 1–3. In the region left of the lines L_{syn}, L_{asyn} and L_k, only steady states are stable, whereas in the grey shaded region the system always reaches one of the stable limit cycles. In the region in between the system tends eventually towards the stable steady state or one of the possible limit cycles.
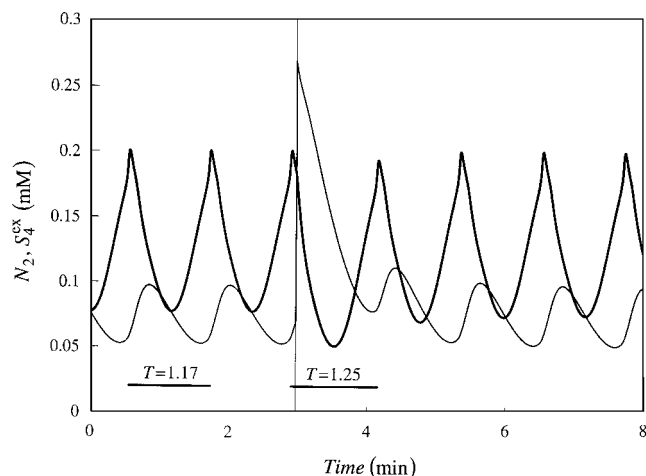
Figure 10   Time course of external acetaldehyde (thin line) and NADH (thicker line) before and after a pulse of 0.2 mM acetaldehyde to the extracellular solution

Parameters: $J_0 = 2.5$ mM · min^{-1}; $k = 1.8$ min^{-1}; reference values for all other parameters. The perturbation is applied at $t = 2.96$ min, which corresponds to $\Phi = 110°$ (cf. Figure 11).

Figure 11   Phase response $\Delta\Psi$ of NADH after addition of a pulse of 0.2 mM acetaldehyde at different Φ values

Parameters: $J_0 = 2.5$ mM · min^{-1}; $k = 1.8$ min^{-1}; reference values for all other parameters. Curve A shows the phase shift after a long time, when the system has returned to the limit cycle; curve B illustrates the phase shift of the first maximum after the perturbation.

$25.0°$. A careful inspection of the time course showed that there was an increase in the phase shift of the following maxima, such that $\Delta\Psi \rightarrow 46.9°$ for very long time periods. Moreover, the addition of acetaldehyde led to a lowering of the first NADH minimum, which was a typical response in experiments [14].

In Figure 11, the phase response $\Delta\Psi$ of NADH after addition of a pulse of 0.2 mM acetaldehyde at different Φ values is shown. Curve A refers to the phase shift ($\Delta\Psi_\infty$) after a long time where the system is returned to the limit cycle, whereas curve B represents the phase shift ($\Delta\Psi_1$) of the first maximum after the
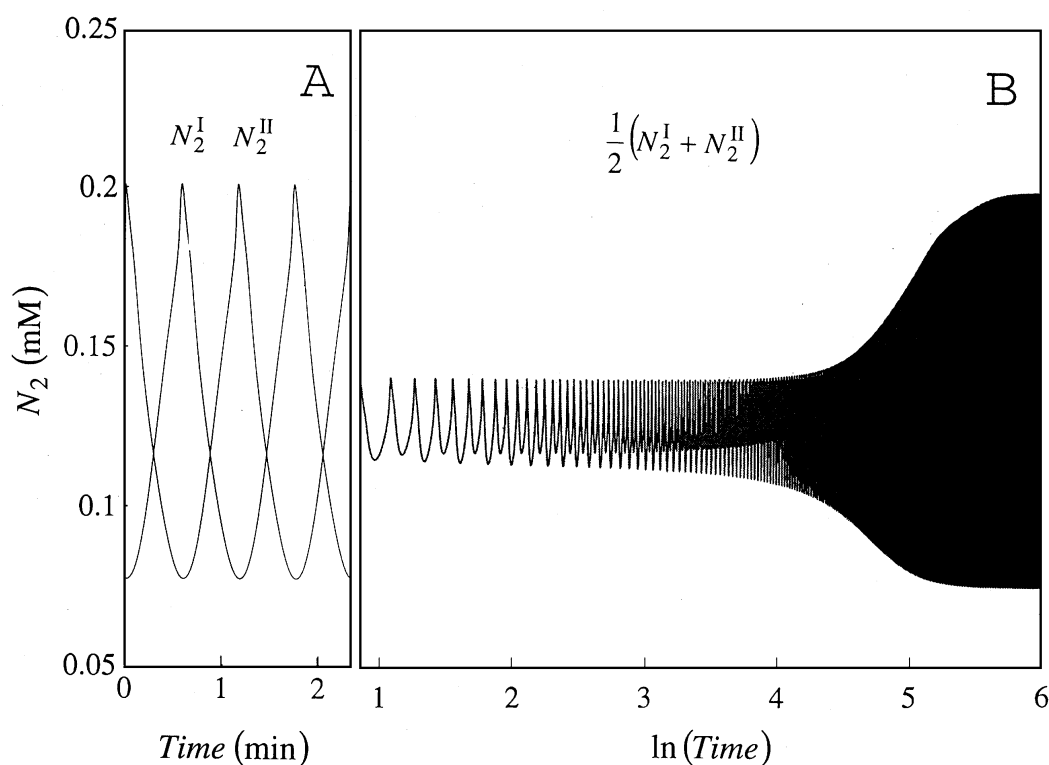
Figure 12   Mixing of two subpopulations

(**A**) Concentrations of NADH in two subpopulations, I and II, oscillating 180° out of phase. (**B**) The mean NADH concentration after mixing of the two subpopulations. The time is shown on a logarithmic scale. Parameters: $J_0 = 2.5$ mM $\cdot$ min^{-1}; $k = 1.8$ min^{-1}; reference values for all other parameters.

Table 3   Control coefficients of the synchronization time for the coupling parameter κ and the combined effect of all other processes

The coefficients were calculated by numerical evaluation of the integrals which enter definition (6) and by analysing the mean effect of an increase and a decrease of the parameters around a reference state by a certain percentage. For the reference set of parameters and with $J_0 = 2.5$ mM $\cdot$ min^{-1} and $k = 1.8$ min^{-1}, the mean synchronization time is $\tau_{syn} = 99.10$ min.

$\Delta p/p$	0.01	0.05	0.10	0.30
$C_{\kappa}^{\tau_{syn}}$	-0.08	-0.07	-0.08	-0.11
$\sum_{p_i \neq \kappa} C_{p_i}^{\tau_{syn}}$	-0.92	-0.93	-0.94	-1.07
$\sum_{p} C_{p}^{\tau_{syn}}$	-1.00	-1.00	-1.02	-1.18

perturbation. Both curves are non-monotonous and have some similarities, i.e. both have maxima for $\Phi \approx 230°$ and $\Phi \approx 350°$. The values of $\Delta\Psi_\infty$ are ubiquitously larger than $\Delta\Psi_1$, indicating that the system does not return to the limit cycle after one period for the given perturbation. In the region $\Phi = 0°$ to $\Phi = 90°$, the shape of curve B differs substantially from that of curve A. In particular, $\Delta\Psi_1$ decreases initially in a much more pronounced manner than $\Delta\Psi_\infty$ at increasing Φ. The curve B has a discontinuity at $\Phi = 90°$, where $\Delta\Psi_1$ jumps from about $-3°$ to values of about $23°$. This effect may be explained as follows: in the region $\Phi = 0°$ to $\Phi = 90°$ of curve B, the NADH concentration increases further after the addition of acetaldehyde, which gives rise to a maximum that follows rather quickly after

the perturbation. However, beyond $\Phi = 90°$ the addition of acetaldehyde is followed by an immediate decrease in the NADH concentration, leading to a delayed occurrence of the next maximum. It is interesting to note that the addition of acetaldehyde immediately before the NADH maximum leads to a phase advance with respect to $\Delta\Psi_1$, but this characteristic vanishes if one considers the phase shift after a long time.

The phase-response curves depicted in Figure 11 show some agreement with experimental data [13], where the first maximum after a pulse was analysed. For example, $\Delta\Psi_1^{exp}$ also decreased in the range $0° < \Phi < 90°$, and increased for $90° < \Phi < 360°$. In the latter region the theoretical value of $\Delta\Psi_1$ increased for $90° < \Phi < 230°$, but decreased thereafter and showed a second maximum at $\Phi \approx 350°$. This very detailed feature of the response could not be seen in experiments which included only a few data points. The absolute values of the phase shifts observed in the experiments are generally higher than those of the model. Moreover, the experimental data indicate that phase shifts are negative in a larger region of Φ than found for curve $\Delta\Psi_1$ in Figure 11.

Mixing of two subpopulations

In order to study the interaction of oscillating cells, simulations were performed where two cell populations I and II are mixed, which are synchronized internally, but oscillate 180° out of phase before mixing. This corresponds to experimental investigations carried out for yeast cells, which show that a rather rapid synchronization occurs after a time which corresponds to 1–2 cycles [11,12] or about 8 cycles [13] of the original limit cycle.

Our model may explain a synchronization of the two sub-

populations via the exchange of acetaldehyde. Figures 12(A) and 12(B) show the simulated concentrations of NADH of two subpopulations before mixing, and the mean NADH concentration after mixing. Immediately after mixing the amplitudes of the mean NADH concentration are strongly damped by a factor of about 5. In the following time course, the amplitudes increase monotonically towards values observed in the two subpopulations before mixing. However, the synchronization time corresponds to about 140 cycles, and it is therefore much longer than in the experiment (please note the logarithmic time scale in Figure 12B). Increasing the coupling parameter κ by a factor of about 100, which strengthens the intercellular communication via transmembrane fluxes of acetaldehyde, decreases the synchronization time only by a factor of about 3. This leads to the conclusion that other processes within this model play a strong role in the limitation of this time (see below).

For a quantitative analysis of the effects of parameters on the synchronization we define a mean synchronization time in the following way:

$$\tau_{syn} = \frac{\int_{t_{mix}}^{\infty} (t - t_{mix}) \cdot |N_2^I - N_2^{II}| dt}{\int_{t_{mix}}^{\infty} |N_2^I - N_2^{II}| dt} \qquad (6)$$

where N_2^I and N_2^{II} denote the concentrations of NADH in the two subpopulations. According to this formula, the mean synchronization time results from a weighting of $t - t_{mix}$, i.e. the times elapsed after mixing, by the differences of the NADH concentrations between the two populations (for general definitions of mean transition times, cf. [20,21]). Variations in the parameters will affect the time courses of N_2^I and N_2^{II} and in this way the synchronization time.

A convenient measure for the parameter dependence of the synchronization time is

$$C_p^{\tau_{syn}} = \frac{\Delta \tau_{syn} / \tau_{syn}}{\Delta p / p} \qquad (7)$$

where p may represent any system parameter. This corresponds to definitions of control coefficients in metabolic control analysis, which have been applied to fluxes and concentrations under steady-state conditions [22], as well as for frequencies and amplitudes of oscillations [23,24]. Our analysis was confined to those parameters p_i that contain the unit of time in the form min^{-1} (see the first nine parameters listed in Table 1). For infinitesimal changes in the parameters, one may derive the summed control of all rates over the mean synchronization time, i.e. the summation relationship, as follows:

$$\sum_i C_{p_i}^{\tau_{syn}} = \sum_i \frac{p_i}{\tau_{syn}} \frac{\partial \tau_{syn}}{\partial p_i} = -1 \qquad (8)$$

Table 3 gives the results of numerical calculations for the control coefficient $C_\kappa^{\tau_{syn}}$ (characterizing the change of τ_{syn} at variations of the coupling flux J), and for the sum of control coefficients of all other processes. This was done for different small but finite changes of the corresponding parameters. It is seen that an increase in κ leads to a decrease in the synchronization time ($C_\kappa^{\tau_{syn}} < 0$). This corresponds to the expectations concerning the role of the coupling flux in the communication between the two cell populations. Surprisingly, the effect of the coupling parameter κ is rather small, although this parameter determines the velocity of the exchange of acetaldehyde. According to Table 3, the synchronization time is limited mainly by the combined effect of all the other processes. This means that a simultaneous increase

Table 4 Control coefficients of the synchronization time for those parameter p_i which have the combined effect listed in Table 3

The parameters were changed by 1%. The sum $\sum_{p_i \neq \kappa} C_{p_i}^{\tau_{syn}}$ results to -0.90, whereas it is -0.92 in Table 3.

Parameter	$C_{p_i}^{\tau_{syn}}$
J_0	$+7.98$
k_1	-1.68
k_2	-7.72
k_3	-2.30
k_4	-0.02
k_5	$+3.61$
k_6	-0.48
k	-0.29

in their rate constants by the same factor leads to an almost proportional decrease in τ_{syn}. For $\Delta p / p \leqslant 0.1$, the summation relationship (eqn. 8) holds true up to the second decimal place. Even for a 30% change of the parameters, the sum deviates only slightly from minus unity.

Calculation of the individual coefficients that have been lumped in Table 3 reveals a very heterogeneous picture concerning the role of the input flux of glucose, and of the intracellular processes in the control of the synchronization time (Table 4). Whereas the combined effect of all parameters is negative, two of the individual control coefficients ($C_{J_0}^{\tau_{syn}}$ and $C_{k_5}^{\tau_{syn}}$) are positive, indicating a prolonged synchronization with a higher influx or an increased rate of the non-glycolytic ATP consumption. Two coefficients are very large in their absolute amounts, but are of opposite sign. This concerns the parameters J_0 and k_2, which have a positive and a negative control coefficient respectively. The coefficient of PFK (reaction 1) is comparatively small, although this enzyme plays a major role in generating the oscillations. Generally, one may conclude that, for synchronization and for generation of oscillations, different processes may be important.

It is difficult to give an intuitive interpretation of the coefficients listed in Table 4, owing to the complexity of the parameter dependence of the non-linear dynamics of two interacting oscillatory systems. The question arises whether there is a relation between the change of the synchronization time and the variation of other global system properties, such as the oscillation period or the mean transmembrane fluxes of the coupling substance. However, a comparison of the effects of parameter changes on the oscillatory period in the model for a single synchronized population showed no direct correlation to the parameter dependence of the mean synchronization time. For example, an increase in J_0 strongly increases the period, whereas an activation of reaction 2 leaves the period nearly unchanged (results not shown).

One would expect that the control coefficient of the transmembrane exchange of the coupling substance would be higher for smaller values of κ. However, in the present case the range of possible values of κ is limited due to a vanishing of the oscillations for $\kappa < 3.2$ min^{-1}.

These results indicate that the proposed synchronization mechanism via acetaldehyde diffusion might not be sufficient to explain the rapid synchronization found in the experiment. In fact, acetaldehyde affects the PFK oscillator only in an indirect way (see Scheme 1). A change in external acetaldehyde will first influence the alcohol dehydrogenase reaction (v_4) and, in this way, the redox state of the cell. This effect is transduced via

reactions 2 and 3 to the concentrations of the adenine nucleotides, which, in turn, modify the PFK reaction. One might expect that the synchronization via acetaldehyde, which affects primarily the lower part of the reaction chain, could be accelerated by introducing regulatory couplings to the upper part of the pathway. This may be one of the many effectors of PFK. Alternative explanations of the rapid synchronization observed in the experiment could be the oscillation of a parameter that modifies the activity of all enzymes, such as pH, or an intercellular communication not only via acetaldehyde, but by a trans-membrane exchange of other intermediates.

DISCUSSION

The investigation of metabolic oscillations in yeast cells has a long tradition concerning glycolytic oscillations with a short period of about 1 min under anaerobic conditions [25,26]. More recently, slower oscillations with a period of about 1 h under aerobic conditions [27,28] have been found. The present study is the first investigation of the interaction of anaerobic, oscillating cells on the basis of a rather detailed description of glycolysis.

A thorough bifurcation analysis of the underlying model combined with numerical simulations shows that, in this multi-variate system, a great variety of dynamical modes exists. Depending on the parameter values, stable steady states, synchronized oscillations, regular asynchronous oscillations and non-regular asynchronous oscillations may occur. In certain parameter regions, the system also displays chaotic behaviour, which we have not studied in detail. Though the model includes many reactions and, therefore, a rather high number of system parameters, only a small number of these parameters have been varied in the bifurcation analysis. These are the input rate of glucose (J_0), the cell density (φ) and the rate constant of the external degradation of the coupling substance (k), since these quantities are amenable to experimental manipulation.

The model results show convincing correspondence to experimental data, in particular that presented in [2]. This concerns the metabolite concentrations, the phase shift between the cellular metabolites in synchronized states, and the existence of a critical range for the input flux and the external degradation rates where oscillations are observed. Furthermore, the model shows a phase response of the synchronized oscillations after addition of acetaldehyde and a synchronization of subpopulations after mixing. There are some quantitative discrepancies between the theoretical results and the experimental data. In particular, the phase response towards changes in the external acetaldehyde concentration is less pronounced in the model, and the simulated synchronization process takes a much longer time. This might indicate that the model is to some extent incomplete. Our assumption that acetaldehyde plays the role of the synchronizing substance is on the basis of that suggested previously [13,14]. These quantitative discrepancies lead us to conclude that coupling via transmembrane exchange of only acetaldehyde may not be sufficient, or that additional internal regulatory couplings have to be taken into account in order to strengthen the signal transduction to the PFK oscillator of a given cell from all surrounding cells.

Obviously, the model may be extended in different ways to cope with the details of yeast cell metabolism. This concerns, for example, the consideration of more realistic rate equations for the individual processes, which would necessitate the consideration of a more complete reaction scheme without any lumping (for a detailed model see [29]). One might expect, however, that these modifications will not change the overall picture of the dynamics.

Using numerical standard procedures, we were able to perform a complete bifurcation analysis for both the single-cell model and for two coupled cells. For the former, the number of system variables is 7, whereas for the latter it is 13. In principle, the program AUTO may be used to treat differential equation systems with a much greater number of variables. Preliminary investigations for three coupled cells lead to much more complex bifurcation diagrams (compared with the case of two cells shown in Figures 3–5). In addition to bifurcations leading to synchronous and regular asynchronous oscillations, further types of non-regular asynchronous oscillations also occur.

One might speculate how the complex bifurcations of two or three cells extrapolate to a macroscopic population. Can regular asynchronous oscillations or more complex limit cycles occur in a population with a large number of cells, or do these phenomena disappear because of averaging? These are questions that should be answered by further research.

The existence of desynchronized oscillations for interacting cells demonstrates that the dynamic behaviour of whole populations, investigated, for example, by the mean values or the time dependence of the extracellular metabolites, may not give a direct indication of the dynamics of the single cell. Non-synchronous oscillations of the individual cells would be characterized by mean concentration values of the population that seem to be constant from a 'macroscopic' point of view. The same holds true for the external concentration of the coupling metabolite. This may give rise to the misleading assumption that the system is in a steady state. Moreover, if such a system is perturbed, for example by addition of metabolites to the external solution, all cells are partly synchronized for a certain period of time. The mean concentration values show damped oscillations, where the damping results from a return to the original phase shifts between the oscillating cells. It would be inappropriate to model such a behaviour as a transition in a stationary state. These phenomena, which have been studied previously for a population of coupled cells containing two-component metabolic oscillators (occurrence of 'hidden oscillations' [15]), are found also in the present model; in particular, for the case of regular asynchronous oscillations. It could well be that oscillatory behaviour on the cellular level is a much more common phenomenon than generally assumed, since on the population level asynchronous oscillations are difficult to distinguish from a stationary behaviour.

REFERENCES

1 Goldbeter, A. (1996) Biochemical Oscillations and Cellular Rhythms: the Molecular Basis of Periodic and Chaotic Behaviour, Cambridge University Press
2 Richard, P., Teusink, B., Hemker, M. B., van Dam, K. and Westerhoff, H. V. (1996) Yeast **12**, 731–740
3 Higgins, J. (1964) Proc. Natl. Acad. Sci. U.S.A. **51**, 989–994
4 Sel'kov, E. E. (1968) Eur. J. Biochem. **4**, 79–86
5 Goldbeter, A. and Lefever, R. (1972) Biophys. J. **12**, 1302–1315
6 Richter, O., Betz, A. and Giersch, C. (1975) Biosystems **7**, 137–146
7 Termonia, Y. and Ross, J. (1981) Proc. Natl. Acad. Sci. U.S.A. **78**, 2952–2956
8 Smolen, P. (1995) J. Theor. Biol. **174**, 137–148
9 Tornheim, K. (1979) J. Theor. Biol. **79**, 491–541
10 Aon, M. A., Cortassa, S., Westerhoff, H. V. and van Dam, K. (1992) J. Gen. Microbiol. **138**, 2219–2227
11 Pye, E. K. (1969) Can. J. Bot. **47**, 271–285
12 Ghosh, A. K., Chance, B. and Pye, E. K. (1971) Arch. Biochem. Biophys. **145**, 319–331

13 Richard, P., Bakker, B. M., Teusink, B., van Dam, K. and Westerhoff, H. V. (1996) Eur. J. Biochem. **235**, 238–241
14 Betz, A. and Becker, J. U. (1975) J. Interdiscip. Cycle Res. **6**, 167–173
15 Wolf, J. and Heinrich, R. (1997) BioSystems **43**, 1–24
16 Doedel, E. J. (1981) Congr. Num. **30**, 265–284
17 Heinrich, R., Rapoport, S. M. and Rapoport, T. A. (1977) Prog. Biophys. Mol. Biol. **32**, 1–82
18 Aldridge, J. and Pye, E. K. (1976) Nature (London) **259**, 670–671
19 Richard, P., Diderich, J. A., Bakker, B. M., Teusink, B., van Dam, K. and Westerhoff, H. V. (1994) FEBS Lett. **341**, 223–226
20 Heinrich, R. and Rapoport, T. A. (1975) BioSystems **7**, 130–136
21 Llorens, M., Nuño, J. C., Rodríguez, Y., Meléndez-Hevia, E. and Montero, F. (1999) Biophys. J. **77**, 23–36
22 Heinrich, R. and Schuster, S. (1996) The Regulation of Cellular Systems, Chapman and Hall, New York
23 Baconnier, P. F., Pachot, P. and Demongeot, J. (1993) J. Biol. Syst. **1**, 335–347
24 Teusink, B., Bakker, B. M. and Westerhoff, H. V. (1996) Biochim. Biophys. Acta **1275**, 204–212
25 Ghosh, A. K. and Chance, B. (1964) Biochem. Biophys. Res. Commun. **16**, 174–181
26 Hess, B. and Boiteux, A. (1968) Hoppe-Seyler's Z. Physiol. Chem. **349**, 1567–1574
27 Satroutdinov, A. D., Kuriyama, H. and Kobayashi, H. (1992) FEMS Microbiol. Lett. **98**, 261–268
28 Keulers, M., Satroutdinov, A. D., Suzuki, T. and Kuriyama, H. (1996) Yeast **12**, 673–682
29 Rizzi, M., Baltes, M., Theobald, U. and Reuss, M. (1997) Biotechnol. Bioeng. **55**, 592–608

APPENDIX A

Metabolic concentrations in the symmetric steady state

In the symmetric steady state the sets of stationary metabolite concentrations are the same in all cells and, moreover, identical with the case of a single cell. Therefore, one may omit the cell index α for the characterization of the cell in eqns. (1)–(4). Despite the non-linearity of the algebraic steady-state equations, an explicit solution may be found which reads:

$$\bar{S}_1 = \frac{J_0}{k_1 \bar{A}_3 f(\bar{A}_3)} \tag{A1}$$

$$\bar{S}_2 = \frac{k_5 \bar{A}_3(k_6 - k_2) + 2J_0(k_2 + k_6)}{2k_2 k_6 N} \tag{A2}$$

$$\bar{S}_3 = \frac{k_5 \bar{A}_3 + 2J_0}{2k_3 \bar{A}_2} \tag{A3}$$

$$\bar{S}_4 = \frac{k_5 \bar{A}_3[k_5 \bar{A}_3(k_6 - k_2) + 2J_0(k_2 + k_6)]}{k_2 k_4 N(2J_0 - k_5 \bar{A}_3)} \tag{A4}$$

$$\bar{N}_1 = \frac{k_6 N(k_5 \bar{A}_3 + 2J_0)}{k_5 \bar{A}_3(k_6 - k_2) + 2J_0(k_2 + k_6)} \tag{A5}$$

$$\bar{S}_4^{\text{ex}} = \frac{k_5^2 \bar{A}_3^2[2\kappa(k_6 - k_2) - k_2 k_4 N] + 4k_5 J_0 \bar{A}_3}{[\kappa(k_2 + k_6) + k_2 k_4 N] - 4k_2 k_4 J_0^2 N}{2k_2 k_4 \kappa N(2J_0 - k_5 \bar{A}_3)} \tag{A6}$$

In these equations the steady-state concentration of ATP is determined by

$$k = \frac{k_2 k_4 \kappa \varphi N(2J_0 - k_5 \bar{A}_3)^2}{4k_5 J_0 \bar{A}_3[\kappa(k_2 + k_6) + k_2 k_4 N] - k_5^2 \bar{A}_3^2} \frac{}{[2\kappa(k_2 - k_6) + k_2 k_4 N] - 4k_2 k_4 J_0^2 N} \tag{A7}$$

which may be rewritten as a quadratic equation for $\bar{A}_3$. It is easy to show that only one of the two solutions leads to non-negative values of the stationary metabolite concentrations.

APPENDIX B

Factorization of the characteristic polynomial for *n* coupled cells

Let us consider n identical cells, each containing a reaction system with m variable metabolites $S_1, \ldots, S_m$. The cells are coupled by the diffusion of one of these substances, e.g. S_m. The system dynamics is described by:

with $\alpha = 1, \ldots, n$; $i, j = 1, \ldots, m$

$$\frac{dS_i^\alpha}{dt} = f_i(S_i^\alpha) - \delta_{im} \kappa(S_m^\alpha - S_m^{\text{ex}}) \tag{B1}$$

$$\frac{dS_m^{\text{ex}}}{dt} = \frac{\kappa\varphi}{n}\left(\sum_{\alpha=1}^{n} S_m^\alpha - nS_m^{\text{ex}}\right) - g(S_m^{\text{ex}}) \tag{B2}$$

where the functions f_i describe the rates of the reactions producing and degrading the internal substances, S_i. $g(S_m^{\text{ex}})$ denotes the degradation rate of the coupling substance S_m^{ex} in the external medium and δ_{im} is the Kronecker symbol ($\delta_{im} = 1$ for $i = m$ and $\delta_{im} = 0$ for $i \neq m$); see eqns. (1)–(4) for the case of yeast glycolysis. The total number of variables in eqn. system (B1) and (B2) amounts to $(m \cdot n + 1)$.

In the following, we use the concentrations S_i^1 of the first cell, the external concentration S_m^{ex} of the coupling substance and the concentration differences:

$$\Delta S_i^\alpha = S_i^\alpha - S_i^1 \text{ with } \alpha = 2, \ldots, n \tag{B3}$$

as a new complete set of variables. The symmetric steady state is characterized by equal concentrations of corresponding metabolites in different cells; that is, by $\overline{S_i^1}$, $\overline{S_m^{\text{ex}}}$ and $\overline{\Delta S_i^\alpha} = 0$. For the stability analysis of this steady state, we consider a linearization of the differential equation system (B1) and (B2) in the neighbourhood of this stationary state with respect to the deviations $\sigma_i^1 = S_i^1 - \overline{S_i^1}$, $\Delta_i^\alpha = \Delta S_i^\alpha - \overline{\Delta S_i^\alpha}$ and $\sigma_m^{\text{ex}} = S_m^{\text{ex}} - \overline{S_m^{\text{ex}}}$. In this way, one obtains for the variables of the first cell:

$$\frac{d\sigma_i^1}{dt} = \sum_{j=1}^{m} \frac{\partial f_i}{\partial S_j^1} \sigma_j^1 - \delta_{im} \kappa(\sigma_m^1 - \sigma_m^{\text{ex}}) \tag{B4}$$

and for the concentration differences characterizing the variables of the other cells $\alpha > 1$:

$$\frac{d\Delta_i^\alpha}{dt} = \sum_{j=1}^{m} \frac{\partial f_i}{\partial S_j^1} \Delta_i^\alpha - \delta_{im} \kappa\Delta_m^\alpha \tag{B5}$$

In the latter equation system, the identity of the cells is taken into account; that is, the derivatives $\partial f_i/\partial S_j^\alpha = \partial f_i/\partial S_j^1$ at the symmetric steady state are, for all values of i and j, independent of the cell index α. Linearization of eqn. (B2) for the concentration of the external metabolite yields:

$$\frac{d\sigma_m^{\text{ex}}}{dt} = \frac{\kappa\varphi}{n}\left(n\sigma_m^1 + \sum_{\alpha=2}^{n} \Delta_m^\alpha - n\sigma_m^{\text{ex}}\right) - \frac{\partial g}{\partial S_m^{\text{ex}}} \sigma_m^{\text{ex}} \tag{B6}$$

Introducing the mean values of the metabolite concentrations:

$$\tilde{S}_i = \frac{1}{n}\sum_{\alpha=1}^{n} S_i^{\alpha}, i = 1,\ldots,m \tag{B7}$$

and the corresponding deviations from their steady-state values $\tilde{\bar{S}}_i$

$$\tilde{\sigma}_i = \tilde{S}_i - \tilde{\bar{S}}_i = \frac{1}{n}\left(n\sigma_i^1 + \sum_{\alpha=2}^{n} \Delta_i^{\alpha}\right) \tag{B8}$$

one derives by taking into account eqns. (B4) and (B5):

$$\frac{\mathrm{d}\tilde{\sigma}_i}{\mathrm{d}t} = \frac{1}{n}\sum_{j=1}^{m} \frac{\partial f_i}{\partial S_j^1}\left(n\sigma_j^1 + \sum_{\alpha=2}^{n} \Delta_j^{\alpha}\right) - \frac{\delta_{im}\kappa}{n}\left(n\sigma_m^1 + \sum_{\alpha=2}^{n} \Delta_m^{\alpha} - n\sigma_m^{\mathrm{ex}}\right) \tag{B9}$$

With eqn. (B8), this equation may be rewritten as:

$$\frac{\mathrm{d}\tilde{\sigma}_i}{\mathrm{d}t} = \sum_{j=1}^{m} \frac{\partial f_i}{\partial S_j^1}\tilde{\sigma}_j - \delta_{im}\kappa(\tilde{\sigma}_m - \sigma_m^{\mathrm{ex}}) \tag{B10}$$

Similarly, one obtains from eqns. (B6) and (B8):

$$\frac{\mathrm{d}\sigma_m^{\mathrm{ex}}}{\mathrm{d}t} = \kappa\varphi(\tilde{\sigma}_m - \sigma_m^{\mathrm{ex}}) - \frac{\partial g}{\partial S_m^{\mathrm{ex}}}\sigma_m^{\mathrm{ex}} \tag{B11}$$

The linear equation system (B10) and (B11) for the deviations $\tilde{\sigma}_i$ of the mean intracellular concentrations, and for the deviation σ_m^{ex} of the extracellular concentration of the coupling substance, is identical with the linearized system of a single cell, containing the same metabolic system. In particular, it is decoupled from the linear equation system (B5) for the differences Δ_i^{α}. Similarly, equation system (B5) for the concentration differences is independent of the mean values. In addition to that, each subsystem of (B5) characterized by a given value of α is decoupled from all other subsystems. These properties imply a factorization of the characteristic polynomial for the eigenvalues in the following way:

$$F(\lambda) \cdot D(\lambda)^{n-1} = 0,$$

where $F(\lambda)$ is the characteristic polynomial of degree $(m+1)$ of the single cell and $D(\lambda)$ the characteristic polynomial of degree m for any subsystem of the linear equation system (B5).